Liu *et al.*
Chinese Journal of Mechanical Engineering (2024) 37:21
https://doi.org/10.1186/s10033-024-00996-9

Chinese Journal of Mechanical Engineering

ORIGINAL ARTICLE

Open Access

Type Synthesis of Self-Alignment Parallel Ankle Rehabilitation Robot with Suitable Passive Degrees of Freedom

Ya Liu[1,2], Wenjuan Lu[2,3,4], Dabao Fan[2], Weijian Tan[2], Bo Hu[1] and Daxing Zeng[2,3,4*]

Abstract

The current parallel ankle rehabilitation robot (ARR) suffers from the problem of difficult real-time alignment of the human-robot joint center of rotation, which may lead to secondary injuries to the patient. This study investigates type synthesis of a parallel self-alignment ankle rehabilitation robot (PSAARR) based on the kinematic characteristics of ankle joint rotation center drift from the perspective of introducing "suitable passive degrees of freedom (DOF)" with a suitable number and form. First, the self-alignment principle of parallel ARR was proposed by deriving conditions for transforming a human-robot closed chain (HRCC) formed by an ARR and human body into a kinematic suitable constrained system and introducing conditions of "decoupled" and "less limb". Second, the relationship between the self-alignment principle and actuation wrenches (twists) of PSAARR was analyzed with the velocity Jacobian matrix as a "bridge". Subsequently, the type synthesis conditions of PSAARR were proposed. Third, a PSAARR synthesis method was proposed based on the screw theory and type of PSAARR synthesis conducted. Finally, an HRCC kinematic model was established to verify the self-alignment capability of the PSAARR. In this study, 93 types of PSAARR limb structures were synthesized and the self-alignment capability of a human-robot joint axis was verified through kinematic analysis, which provides a theoretical basis for the design of such an ARR.

Keywords Ankle rehabilitation robot, Self-alignment, Parallel mechanism, Type synthesis, Screw theory

1 Introduction

The incidence of stroke gradually increases as aging progresses and many patients suffer from lower-extremity motor dysfunction owing to foot drop [1]. Medical research has indicated that effective rehabilitation training can accelerate the healing of damaged tissues, restore ligament elasticity, prevent joint adhesion, maintain joint flexibility, and accelerate joint rehabilitation, enabling patients to return to normal exercise performance quickly [2, 3]. Numerous studies have acknowledged the accurate work of rehabilitation physicians who perform a number of exercises significantly better than robots. However, the increasing number of patients and lack of medical personnel have driven a paradigm shift in rehabilitation. Thus, improved solutions are necessary to achieve faster recovery while simultaneously treating multiple patients [4]. To address this issue, ankle rehabilitation robots (ARRs) have been developed to reduce the labor intensity of rehabilitation physicians.

An ARR assists patients in rehabilitation exercise training and has many advantages compared to the traditional manual rehabilitation training modes, including: (i) ensuring the intensity, effect, and precision of

*Correspondence:
Daxing Zeng
zengdx@dgut.edu.cn
[1] School of Mechanical Engineering, Yanshan University, Qinhuangdao 066004, China
[2] School of Mechanical Engineering, Dongguan University of Technology, Dongguan 523808, China
[3] Dongguan Engineering Technology Research Center for Parallel Robot, Dongguan 523808, China
[4] The DGUT Innovation Center of Robotics and Intelligent Equipment, Dongguan 523808, China

rehabilitation training and better consistency of movement [5]; (ii) providing personalized training with different intensities and modes according to the degree of injury and rehabilitation of patients, and enhancing active participation of patients [6]; and (iii) quantitatively evaluating the rehabilitation progress of patients and providing a basis for improving the rehabilitation treatment scheme [7]. However, ARRs currently have problems, such as poor flexibility and low safety. Therefore, the research regarding ARRs has attracted increasing attention.

ARRs can be classified into two types according to their structures: platform and wearable robots [8]. Wearable robots have been used for gait rehabilitation training [9]. Platform robots can perform complex and specialized spatial motions, and are used to assist patients with physical disabilities or mobility difficulties during rehabilitation. They aid in preventing joint stiffness and improving joint range of motion and ankle proprioception [10]. Among platform ARRs, parallel ARRs have received wide attention because of their advantages, such as small inertia, high stiffness, compact structure, and high precision [11, 12].

Dai et al. [13] developed several ARRs using 3-SPS/S and 3-SPS/SP parallel mechanisms as the main structures. Saglia et al. [14] developed a two degrees of freedom (DOF) ARR controlled by three linear actuators. Ai et al. [15] developed a two DOF parallel-compliant ARR actuated by pneumatic muscles. Tsoi et al. [16, 17] developed an ARR that did not set a rotational axis to assist the rotation of the moving platform. Therefore, the subjects needed to control the lower limb as the rotation support and the ankle as the rotation center during rehabilitation training. Jamwal et al. [18, 19] proposed a lightweight and compliant parallel ARR in which pneumatic muscle actuators were placed parallel to the shinbone of the patient. Zou et al. [20] proposed a 3-RRS parallel ARR that could realize single and compound ankle rehabilitation training. Zhang et al. [21] and Qian et al. [22] developed ARRs driven by pneumatic muscle actuators that could realize changes in motion and dynamic performance by reconfiguring the actuator layouts. Li et al. [23, 24] and Dong et al. [25] presented novel parallel ARRs with the key characteristics of a simple configuration and no actuator redundancy. Liu et al. [26] designed a compliant ankle-rehabilitation robot redundantly driven by pneumatic muscles and cables to provide full range of motion and torque ability for the human ankle. Abu-Dakka et al. [27] developed a 3-PRS parallel ARR with three DOF that realized dorsiflexion (DO)/plantarflexion (PL), inversion (IN)/eversion (EV), and translation in the height direction. Zhang et al. [28] and Liu et al. [29] proposed compact generalized spherical parallel mechanisms suitable for ankle rehabilitation based on an ankle-motion fitting model with a high matching degree. Zeng et al. [30] proposed a new type of ankle-foot rehabilitation robot based on a decoupling series-parallel mechanism with one translational and three rotational DOF. Liu et al. [31] proposed a multi-locomotion-mode ARR based on a 2-UPU/RPU parallel mechanism that supported the training of muscle groups and ligaments related to ankle motion in addition to the rehabilitation training of the basic motion orientation of the ankle.

The aforementioned parallel ARR can be divided into two categories according to the relative positional relationship between the actuators and end effector: actuators below the end effector (AbEE) and actuators above the end effector (AaEE). The driving directions of ARRs with AaEE and the ankle were similar, providing a more suitable motion of the moving platform for the human ankle. However, a common problem between the two types of ARRs is that the mechanical axis of the rehabilitation robot is difficult to align or it coincides with the ankle joint axis/center in real time [32]. This, in turn, leads to human-robot motion incompatibility that results in secondary injury to the patient and is prevalent in joint rehabilitation robots. Several studies have been conducted to address this issue.

Niu et al. [33] proposed a compliant five-bar parallel mechanism that offered two mobilities in the sagittal plane. Additionally, the torsional springs mounted on this mechanism had the potential to automatically adjust the instantaneous center of rotation of the output link connected to the thigh with respect to the basis link connected to the shank. Sarkisian et al. [34, 35] proposed a novel powered knee exoskeleton with a self-alignment mechanism using a prismatic-revolute-revolute (PRR) configuration. Awad et al. [36] presented a novel approach for solving the self-axis alignment problem of an elbow exoskeleton using a planar parallel mechanism. Sun et al. [37] proposed a novel index finger exoskeleton with three motors to help post-stroke patients perform finger abduction (AB)/adduction (AD) and flexion/extension training. In addition, a spatial mechanism with passive DOF for the metacarpophalangeal joint was designed to realize human-robot axes self-alignment. Li et al. [38, 39] developed an upper-limb rehabilitation exoskeleton that achieved kinematic compatibility between the exoskeleton mechanism and human upper arm by introducing passive kinematic pairs. Trigili et al. [40] presented the design and experimental characterization of a four-DOF shoulder-elbow exoskeleton for upper-limb neurorehabilitation and treatment of spasticity that employed a self-alignment mechanism based on passive rotational joints to smoothly self-align the robot's rotational axes to the axes of the user.

Rehabilitation robots for relatively simple self-aligning uni-/bi-axial joints (knee, elbow, and finger) have been thoroughly studied through analysis and comparison. Current research is mainly focused on series shoulder rehabilitation robots for a self-aligned multi-axis joint (shoulder). More complex joint rehabilitation robots based on parallel mechanisms have rarely been reported because the motion of the moving platform output feature point is realized by coupling more than two limbs, making the configuration design difficult.

To this end, the type synthesis of a self-alignment ankle rehabilitation robot (PSAARR) is researched, focusing on the issue of the human-robot joint axis of the current parallel ARR being difficult to align in real time. The "suitable DOF" is introduced to transform the human-robot closed chain (HRCC) formed by an ARR and human body into a kinematic suitable constrained system. The remainder of this paper is organized as follows. The self-alignment principle of the parallel ARR is described in Section 2, the type synthesis conditions of the PSAARR are presented in Section 3, type synthesis method and process of the PSAARR are described in Section 4, self-alignment capability analysis of the PSAARR is presented in Section 5, and conclusions are drawn in Section 6.

2 Self-Alignment Principle of Parallel ARR

The ankle is composed of tibia, fibula, talus, and calcaneus, which belong to the trochlear joint [41]. Based on the morphological structure and function of the ankle, the basic motion types include DO/PL, IN/EV, and AD/AB [42], as depicted in Figure 1. It is known from human anatomy that there is a coupling relationship between various movements of the ankle joint, and that the ankle joint rotation center drifts as its angle changes. Therefore, the ankle joint is equivalent to a three DOF spherical joint with the characteristics of a rotation center drift.

From the perspective of the mechanism theory, the problem of human-robot kinematic incompatibility is caused by the insufficient DOF of the HRCC, making it difficult for the ARR to adapt to changes in the center of rotation of the ankle joint. Therefore, a suitable number and form of passive DOF must be introduced to transform the HRCC formed by the ARR and human body into a kinematic suitably constrained system. In this study, the passive DOF with a suitable number and form is defined as a "suitable DOF".

The concept of an "equivalent virtual series kinematic chain" for a parallel robot that was proposed by Kong et al. [43] is introduced to simplify the HRCC model. For any parallel robot, the corresponding virtual series kinematic chain can be determined by solving the kinematic space analytical expression for its moving platform. A schematic of the HRCC formed by the human body and equivalent virtual series kinematic chain of the ARR is shown in Figure 1.

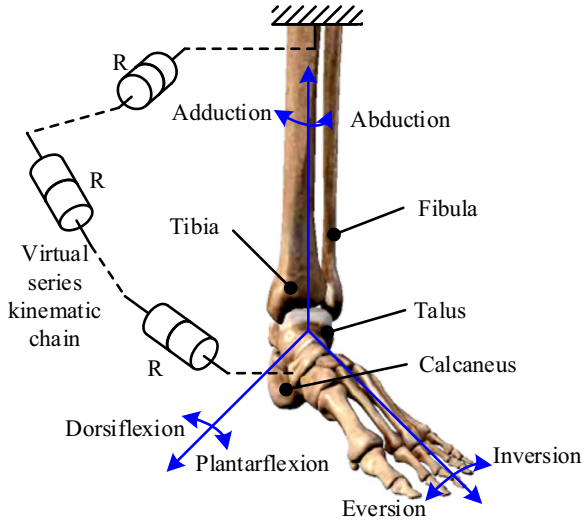

Figure 1 Morphological structure of the ankle joint and its HRCC model

The DOF of the HRCC can be determined using the modified Grübler–Kutzbach criterion [44] as:

$$M = \sum_{i=1}^{g} f_i + 6(n - g - 1) + \mu, \tag{1}$$

where M represents the DOF of the HRCC, f_i represents the DOF of the ith kinematic pair of the HRCC, g represents the number of kinematic pairs of the HRCC, n represents the number of components (including the frame) of the HRCC, and μ represents the number of over constraints of the HRCC. According to "Euler's formula" in the graph theory, $l = g + 1 - n$, and l represents the number of loops of the HRCC.

For the PSAARR, Eq. (1) can be expressed as:

$$M = f_k + f_{uk} - 6l + \mu, \tag{2}$$

where f_k and f_{uk} represent the DOF of the known and unknown kinematic pairs of the HRCC, respectively.

According to the morphological structure and function of the PSAARR HRCC, the DOF of the HRCC is $M = 3$, that is, the DO/PL, IN/EV and AD/AB of the ankle joint. The DOF of the known kinematic pairs is $f_k = 6$, that is, three active kinematic pairs of the PSAARR and three DOF of the ankle joint. The number of loops is $l = 1$ and the number of the over constraint is $\mu = 0$. Therefore, the DOF of unknown kinematic pairs f_{uk} can be solved using Eq. (2).

$$f_{uk} = M - f_k + 6l - \mu = 3 - 6 + 6 \times 1 - 0 = 3. \tag{3}$$

According to Eq. (3), three passive DOF should be introduced into the HRCC, that is, three translation DOF in mutually perpendicular directions. Therefore, the PSAARR should have six DOF, including three active DOF of rotation (moving platform orientation) and three passive DOF of translation (moving platform position). The three active DOF of rotation are controlled by the three driving pairs, and the three passive DOF of translation are controlled by the human body to achieve the self-alignment of the human-robot axis.

Simultaneously, active and passive DOF are required to be decoupled (be in a "decoupled" condition) to ensure that active rehabilitation training and passive self-alignment are independent of one other and to avoid mutual interference between them. In addition, the number of limbs should be equal to the number of active DOF to reduce the number of limbs, reduce mutual interference of limbs, and expand the workspace of the robot. This is known as the "less limb" condition. Based on this, a three-limb six-DOF rotation and translation decoupled parallel mechanism was proposed as the main structure of the PSAARR.

In summary, a self-alignment principle of parallel ARR was proposed that included:

(i) Three "suitable passive DOF" of translation that are based on three active DOF of rotation, such that the HRCC formed by the rehabilitation robot and human body was transformed into a kinematic suitable constraint system.

(ii) Active and passive DOF that are decoupled, and a number of limbs that was equal to the number of active DOF.

3 Type Synthesis Conditions of the PSAARR

The velocity Jacobian matrix of the parallel robot represents the velocity transfer relationship between the operational and joint spaces. The velocity Jacobian matrix of a PSAARR has a specific form according to the self-alignment principle. The relationship between the velocity Jacobian matrix of the PSAARR and its actuation wrenches (the twists) can be established based on the screw theory. Thus, the relationship between the self-alignment principle of the parallel ARR and the actuation wrenches (the twists) of the PSAARR can be established with the velocity Jacobian matrix as "the bridge".

3.1 Velocity Jacobian Matrix Form of PSAARR

The relationship between the joint space velocity $\dot{\boldsymbol{q}}$, velocity Jacobian matrix $\boldsymbol{J}$, and operating space velocity $\dot{\boldsymbol{X}}$ for a parallel robot is $\dot{\boldsymbol{q}} = \boldsymbol{J}\dot{\boldsymbol{X}}$.

For the PSAARR:

(i) Joint space velocity $\dot{\boldsymbol{q}}$ of the limbs can be expressed as:

$$\dot{\boldsymbol{q}} = \left(\dot{q}_{11} \;\; \dot{q}_{12} \;\; \dot{q}_{21} \;\; \dot{q}_{22} \;\; \dot{q}_{31} \;\; \dot{q}_{32} \right)^{\mathrm{T}}, \tag{4}$$

where $\dot{q}_{ij}$ represents the velocity of the jth kinematic pair of ith limb. The active kinematic pairs q_{i1} (main active) and q_{i2} (subactive) control the rotation and translation of the moving platform, respectively.

(ii) The operating space velocity $\dot{\boldsymbol{X}}$ is expressed as:

$$\dot{\boldsymbol{X}} = \left(v_X \;\; v_Y \;\; v_Z \;\; \omega_X \;\; \omega_Y \;\; \omega_Z \right)^{\mathrm{T}}, \tag{5}$$

where v_X, v_Y, and v_Z represent the translational velocity components of the operating space. Similarly, ω_X, ω_Y, and ω_Z represent the rotational velocity components of the operating space.

(iii) The velocity Jacobian matrix $\boldsymbol{J}$ is expressed as:

$$\boldsymbol{J} = \left(\boldsymbol{J}_1 \;\; \boldsymbol{J}_2 \;\; \boldsymbol{J}_3 \right)^{\mathrm{T}}, \tag{6}$$

$$\boldsymbol{J}_i = \begin{pmatrix} 0 & 0 & 0 & J_{i14} & J_{i15} & J_{i16} \\ J_{i21} & J_{i22} & J_{i23} & 0 & 0 & 0 \end{pmatrix}, \quad (i = 1,\ 2,\ 3).$$

Eq. (6) represents the velocity Jacobian matrix form of the PSAARR.

3.2 Velocity Jacobian Matrix Analysis of PSAARR

The velocity Jacobian matrix for parallel robots can be analyzed using the screw theory. A typical parallel robot consists of n limbs in which each limb typically has at least one active kinematic pair and the other kinematic pairs are passive. Multi-DOF kinematic pairs must be equated to a combined form of single-DOF kinematic pairs to facilitate characterization. This way, each limb can be regarded as an open-loop kinematic chain composed of several single-DOF kinematic pairs with its end connected to a moving platform.

The instantaneous output motion of a parallel robot moving platform can be represented by a linear combination of instantaneous screw motions in the limbs as:

$$\boldsymbol{v} = \sum_{j=1}^{m_i} \dot{q}_{ij} \$_{ij} = (\$_{i1} \;\; \$_{i2} \;\; \cdots \;\; \$_{im})(\dot{q}_{i1} \;\; \dot{q}_{i2} \;\; \cdots \;\; \dot{q}_{i3})^{\mathrm{T}}, \quad (i = 1,\ 2,\ \cdots,\ n), \tag{7}$$

where $\boldsymbol{v}$ represents the instantaneous output velocity vector at the end of the limb, $\$_{ij}$ represents the instantaneous twist of the jth single-DOF kinematic pair of the ith limb, and m_i represents the degrees of connection of the ith limb.

The actuation wrench represents the active-force screw applied to the moving platform by the driving pair of limbs.

The actuation wrench does not work on the twist corresponding to the passive kinematic pair (referred to as a passive twist) in the same limb, and the reciprocal product of the two is zero. Assuming that there are g active kinematic pairs in each limb, there are at least g reciprocal screws (actuation wrench) that are reciprocal to all passive screws in each limb.

The unit screw of the actuation wrench can be expressed as $\$_{rij}$ (j=1, 2, ..., g), and the passive twist in Eq. (7) can be eliminated using the reciprocal screw theory. The orthogonal operation on both sides of Eq. (7) with $\$_{rij}$ yields the following relationship:

$$\boldsymbol{J}_{Xi}\dot{\boldsymbol{X}} = \boldsymbol{J}_{qi}\dot{\boldsymbol{q}}_i \quad (i = 1,\ 2,\ \cdots,\ n). \tag{8}$$

In Eq. (8),

$$\boldsymbol{J}_{Xi} = \begin{pmatrix} \$_{ri1} & \$_{ri2} & \cdots & \$_{rig} \end{pmatrix}^{\mathrm{T}},$$

$$\boldsymbol{J}_{qi} = \begin{pmatrix} \$_{ri1}\circ\$_{i1} & \$_{ri1}\circ\$_{i2} & \cdots & \$_{ri1}\circ\$_{ig} \\ \$_{ri2}\circ\$_{i1} & \$_{ri2}\circ\$_{i2} & \cdots & \$_{ri2}\circ\$_{ig} \\ \vdots & \vdots & & \vdots \\ \$_{rig}\circ\$_{i1} & \$_{rig}\circ\$_{i2} & \cdots & \$_{rig}\circ\$_{ig} \end{pmatrix},$$

$$\dot{\boldsymbol{q}}_i = \begin{pmatrix} \dot{q}_{i1} & \dot{q}_{i2} & \cdots & \dot{q}_{ig} \end{pmatrix}^{\mathrm{T}}.$$

Eq. (8) contains n equations, written in matrix form as:

$$\boldsymbol{J}_X\dot{\boldsymbol{X}} = \boldsymbol{J}_q\dot{\boldsymbol{q}}, \tag{9}$$

$$\boldsymbol{J}_X = \begin{pmatrix} \boldsymbol{J}_{X1} & \boldsymbol{J}_{X2} & \cdots & \boldsymbol{J}_{Xn} \end{pmatrix}^{\mathrm{T}},$$

$$\boldsymbol{J}_q = \begin{pmatrix} \boldsymbol{J}_{q1} & \boldsymbol{0} & \cdots & \boldsymbol{0} \\ \boldsymbol{0} & \boldsymbol{J}_{q2} & \cdots & \boldsymbol{0} \\ \vdots & \vdots & & \vdots \\ \boldsymbol{0} & \boldsymbol{0} & \boldsymbol{0} & \boldsymbol{J}_{qn} \end{pmatrix},$$

where $\boldsymbol{J}_X$ and $\boldsymbol{J}_q$ represent the positive and inverse Jacobian matrices of the parallel robot, respectively.

According to Eq. (9), if the inverse Jacobian matrix $\boldsymbol{J}_q$ is a full-rank matrix, then:

$$\dot{\boldsymbol{q}} = \boldsymbol{J}_q^{-1}\boldsymbol{J}_X\dot{\boldsymbol{X}} = \boldsymbol{J}\dot{\boldsymbol{X}}. \tag{10}$$

The positive Jacobian matrix $\boldsymbol{J}_X$ of the three-limb six-DOF parallel robot is expressed as:

$$\boldsymbol{J}_X = \begin{pmatrix} \boldsymbol{J}_{X1} & \boldsymbol{J}_{X2} & \boldsymbol{J}_{X3} \end{pmatrix}^{\mathrm{T}}, \tag{11}$$

$$\boldsymbol{J}_{Xi} = \begin{pmatrix} \$_{ri1} & \$_{ri2} \end{pmatrix}^{\mathrm{T}}, \quad (i = 1,\ 2,\ 3).$$

The inverse Jacobian matrix $\boldsymbol{J}_q$ of the three-limb six-DOF parallel robot is expressed as:

$$\boldsymbol{J}_q = \begin{pmatrix} \boldsymbol{J}_{q1} & \boldsymbol{0} & \boldsymbol{0} \\ \boldsymbol{0} & \boldsymbol{J}_{q2} & \boldsymbol{0} \\ \boldsymbol{0} & \boldsymbol{0} & \boldsymbol{J}_{q3} \end{pmatrix}, \tag{12}$$

$$\boldsymbol{J}_{qi} = \begin{pmatrix} J_{qi11} & J_{qi12} \\ J_{qi21} & J_{qi22} \end{pmatrix} = \begin{pmatrix} \$_{ri1}\circ\$_{i1} & \$_{ir1}\circ\$_{i2} \\ \$_{ri2}\circ\$_{i1} & \$_{ri2}\circ\$_{i2} \end{pmatrix}, \quad (i = 1,\ 2,\ 3).$$

According to Eqs. (10), (11), and (12), the velocity Jacobian matrix $\boldsymbol{J}$ can be expressed as:

$$\boldsymbol{J} = \begin{pmatrix} \boldsymbol{J}_1 \\ \boldsymbol{J}_2 \\ \boldsymbol{J}_3 \end{pmatrix} = \begin{pmatrix} \boldsymbol{J}_{q1}^{-1} & \boldsymbol{0} & \boldsymbol{0} \\ \boldsymbol{0} & \boldsymbol{J}_{q2}^{-1} & \boldsymbol{0} \\ \boldsymbol{0} & \boldsymbol{0} & \boldsymbol{J}_{q3}^{-1} \end{pmatrix} \begin{pmatrix} \boldsymbol{J}_{X1} \\ \boldsymbol{J}_{X2} \\ \boldsymbol{J}_{X3} \end{pmatrix}. \tag{13}$$

The instantaneous twist of the single-DOF kinematic pair $\$_{ij}$ can be expressed as:

$$\begin{aligned} \$_{ij} &= \begin{pmatrix} L_{ij} & M_{ij} & N_{ij} & ; & P_{ij} & Q_{ij} & R_{ij} \end{pmatrix}, \\ (i = 1,\ 2,\ 3), &\quad (j = 1,\ 2,\ \cdots,\ 6), \end{aligned} \tag{14}$$

where $\$_{ij}$ represents the active and passive kinematic pair twists when j = 1, 2 and j = 3, 4, 5, 6, respectively.

The actuation wrench $\$_{rij}$ can be expressed as:

$$\begin{aligned} \$_{rij} &= \begin{pmatrix} L_{rij} & M_{rij} & N_{rij} & ; & P_{rij} & Q_{rij} & R_{rij} \end{pmatrix}, \\ &(i = 1,\ 2,\ 3), \quad (j = 1,\ 2). \end{aligned} \tag{15}$$

Combining Eqs. (13) – (15) results in:

$$\boldsymbol{J}_i = \boldsymbol{J}_{i1}\boldsymbol{J}_{i2}, \quad (i = 1,\ 2,\ 3), \tag{16}$$

$$\boldsymbol{J}_{i1} = \frac{1}{J_{qi11}J_{qi22} - J_{qi12}J_{qi21}} \begin{pmatrix} J_{qi22} & -J_{qi21} \\ -J_{qi12} & J_{qi11} \end{pmatrix},$$

$$\boldsymbol{J}_{i2} = \begin{pmatrix} L_{ri1} & M_{ri1} & N_{ri1} & P_{ri1} & Q_{ri1} & R_{ri1} \\ L_{ri2} & M_{ri2} & N_{ri2} & P_{ri2} & Q_{ri2} & R_{ri2} \end{pmatrix}.$$

Eq. (16) represents the relationship between the velocity Jacobian matrix and limb actuation wrench (and twist) of the PSAARR.

3.3 Condition of Actuation Wrench and Twist

According to the screw theory, the actuation wrench in the same limb works on the corresponding actuated twist, and the reciprocal product of the two cannot be zero. Therefore, J_{qi11} and J_{qi22} in Eq. (16) were not zero. Subsequently, the main active q_{i1} and subactive q_{i2} kinematic pairs control the rotation and translation

of the moving platform, respectively. Thus, the actuation wrenches $\$_{ri1}$ and $\$_{ri2}$ that correspond to the main active q_{i1} and subactive q_{i2} kinematic pairs were a zero (or infinite) pitch screw and a zero-pitch screw, respectively. This results in L_{ri2}, M_{ri2}, and N_{ri2} in Eq. (16) not being zero at the same time.

Combining Eqs. (6) and (16) results in:

$$\begin{cases} J_{qi12} = J_{qi21} = 0, \\ L_{ri1}{=}M_{ri1}{=}N_{ri1}{=}0, \\ P_{ri2}{=}Q_{ri2}{=}R_{ri2}{=}0. \end{cases} \tag{17}$$

According to Eq. (17), the actuation wrench can be expressed as:

$$\begin{cases} \$_{ri1}{=}\left(0\ 0\ 0\ ;\ P_{ri1}\ \ Q_{ri1}\ \ R_{ri1}\right), \\ \$_{ri2} = \left(L_{ri2}\ \ M_{ri2}\ \ N_{ri2}\ ;\ 0\ 0\ 0\right). \end{cases} \tag{18}$$

According to Eq. (18), the actuation wrench $\$_{ri1}$ is an infinite pitch screw and the actuation wrench $\$_{ri2}$ is a zero pitch screw passing through the coordinate origin.

Combining the nature of the reciprocity between the actuation wrench and passive twist yields:

$$\begin{cases} \$_{ri1} \circ \$_{ij} = 0 \quad (j = 2,\ 3,\ 4,\ 5,\ 6), \\ \$_{ri2} \circ \$_{ij} = 0 \quad (j = 1,\ 3,\ 4,\ 5,\ 6). \end{cases} \tag{19}$$

According to Eq. (19), the following condition for a PSAARR should be satisfied: In the same limb, the reciprocal product of the actuation wrench and all other twists is zero, except for the corresponding twist.

4 Type Synthesis Method and Process of the PSAARR

4.1 Type Synthesis Method of the Limb

The kinematic output characteristics of the parallel robot moving platform were determined using the kinematic pair type, number, order, and configuration of each limb, and the assembly form between the limbs. Limb-type synthesis is the key link, theoretical basis, and prerequisite for realizing parallel robot-type synthesis. The limb-type synthesis method and specific steps of the PSAARR were as follows:

(i) All the possible forms of passive twist were determined based on the reciprocal product of the actuation wrench and passive twist in the same limb being zero.

(ii) All possible forms of the active twist were determined based on the reciprocal product of the actuation wrench and corresponding active twist not being zero, and the reciprocal product of the actuation wrench and non-corresponding active twist being zero.

(iii) The feasible number of various twists in the limb was determined based on the maximum linear irrelevance group condition of the twist system.

(iv) The type, number, and configuration orientation of the kinematic pairs in each limb were determined according to the forms of the active and passive twists. Additionally, the existence of an inert pair was considered.

(v) A limb-type synthesis was conducted according to the different degrees of limb connectivity, and all feasible limb structures were listed.

The limb type synthesis process of the PSAARR is shown in Figure 2.

Only the basic kinematic pair was considered for the type synthesis of the limb to simplify the structure and limit space. For the case where the basic kinematic pair was replaced by a composite kinematic pair, refer to Ref. [45].

4.2 Type Synthesis of Passive Kinematic Pair Limb

All possible forms of the passive kinematic pair twist were determined based on the reciprocal product of the actuation wrench and all passive kinematic pair twists in the limb being equal to zero. According to Eq. (18), the passive kinematic pair twist can be expressed as:

$$\begin{cases} \$_{i3} = \left(-Q_{ri1}\ \ P_{ri1}\ \ 0\ ;\ 0\ 0\ 0\right), \\ \$_{i4} = \left(-R_{ri1}\ \ 0\ \ P_{ri1}\ ;\ 0\ 0\ 0\right), \\ \$_{i5} = \left(0\ 0\ 0\ ;\ -M_{ri2}\ \ L_{ri2}\ \ 0\right), \\ \$_{i6} = \left(0\ 0\ 0\ ;\ \ -N_{ri2}\ \ 0\ \ L_{ri2}\right). \end{cases} \tag{20}$$

Other forms of twisting can be obtained using a linear combination of the four twists in Eq. (20). However,

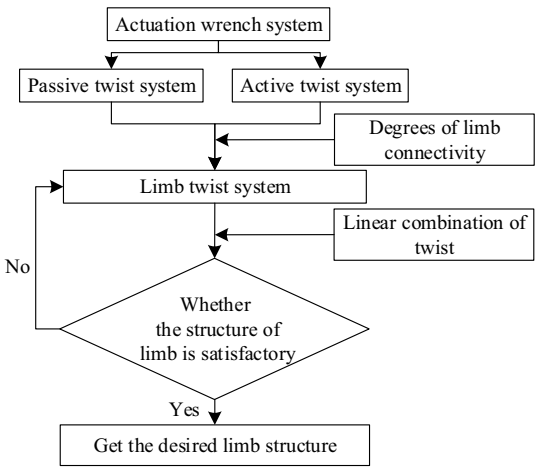

Figure 2 Limb type synthesis process of the PSAARR

the twists after the linear combination must be linearly independent. The case of redundant kinematics in the limb was not considered. That is, only the case in which the connectivity of the passive kinematic pair limb is four was considered. The passive kinematic limb pairs are listed in Table 1.

4.3 Type Synthesis of Active Kinematic Pairs Limb

4.3.1 Type Synthesis of Subactive and Passive Kinematic Pairs

The structures of the subactive and passive kinematic pairs were further determined based on the structure of the passive kinematic pair and according to the condition that the reciprocal product of the subactive kinematic pair twist $\$_{i2}$ and main actuation wrench $\$_{ri1}$ was zero.

According to Eqs. (18) and (20), the twisting system of the subactive and passive kinematic pairs can be expressed as:

Table 1 Passive kinematic pairs of PSAARR

Category	Type	Quantity
2R2P	$\mathrm{PP}\hat{\mathrm{R}}\hat{\mathrm{R}}, \left(\left(\overline{\mathrm{P}}\tilde{\mathrm{P}}\mathrm{R}_1\right)\mathrm{R}\right)$	7
3R1P	$\left(\left(\overline{\mathrm{P}}\mathrm{R}_1\mathrm{R}_1\right)\mathrm{R}\right)$	6
4R	$((\mathrm{R}_1\mathrm{R}_1\mathrm{R}_1)\mathrm{R})$	2

Note: (i) $\hat{\mathrm{R}}$ indicates that the axis of the revolute pair passed through the rotation center of the moving platform. (ii) $\mathrm{R}_1\mathrm{R}_1$ indicates that the axes of the revolute pairs were parallel. (iii) $\overline{\mathrm{P}}$ or $\tilde{\mathrm{P}}$ indicates that the axis of the prismatic pair was perpendicular to the axis of the revolute pair R_1, whereas $\overline{\mathrm{P}}$ and $\tilde{\mathrm{P}}$ were considered as the same element and were not distinguished when sorting. (iv) The elements in ( ) can be arranged and combined arbitrarily. For example, $((\mathrm{R}_1\mathrm{R}_1\mathrm{R}_1)\mathrm{R})$, including $\mathrm{RR}_1\mathrm{R}_1\mathrm{R}_1$ and $\mathrm{R}_1\mathrm{R}_1\mathrm{R}_1\mathrm{R}$. (v) Points (i) to (iv) are equally valid in the following

$$\begin{cases} \$_{i2} = \left(0\ 0\ 0\ ;\ 1\ 0\ 0\right), \\ \$_{i3} = \left(-Q_{ri1}\ P_{ri1}\ 0\ ;\ 0\ 0\ 0\right), \\ \$_{i4} = \left(-R_{ri1}\ 0\ P_{ri1}\ ;\ 0\ 0\ 0\right), \\ \$_{i5} = \left(0\ 0\ 0\ ;\ -M_{ri2}\ L_{ri2}\ 0\right), \\ \$_{i6} = \left(0\ 0\ 0\ ;\ -N_{ri2}\ 0\ L_{ri2}\right). \end{cases} \tag{21}$$

Other forms of twisting can be obtained using a linear combination of the five twists in Eq. (21). However, the twists after the linear combination must be linearly independent. The case of redundant kinematics in the limb was not considered. That is, only the case where the connectivity of the subactive and passive kinematic pair was five was considered. The kinematic pair structures from the obtained twist system whose passive kinematic pairs were according to those listed in Table 1 were selected, as listed in Table 2.

The following conditions must be satisfied for the structure of the subactive and passive kinematic pairs, as listed in Table 2:

(i) The axis direction of the revolute pair must be two.
(ii) The number of revolute pairs in the same direction must be less than four.
(iii) The number of prismatic pairs must be less than four.

4.3.2 Type Synthesis of Main Active and Passive Kinematic Pairs

The structure of the main active and passive kinematic pairs was based on determining the structure of the passive kinematic pair and was further determined according to the condition that the reciprocal product of the main active kinematic pair twist $\$_{i1}$ and subactuation wrench $\$_{ri2}$ was zero.

Table 2 Subactive and passive kinematic pairs of PSAARR

Category	Subactive kinematic pair	Passive kinematic pair	Type	Quantity
2R3P	R_{sa}	Non-existent	Non-existent	0
	P_{sa}	$\mathrm{PP}\hat{\mathrm{R}}\hat{\mathrm{R}}$	$(\mathrm{P}_{sa}\mathrm{PP})\hat{\mathrm{R}}\hat{\mathrm{R}}$	3
		$\left(\left(\overline{\mathrm{P}}\tilde{\mathrm{P}}\mathrm{R}_1\right)\mathrm{R}\right)$	$\left(\left(\dot{\mathrm{P}}_{sa}\overline{\mathrm{P}}\tilde{\mathrm{P}}\mathrm{R}_1\right)\mathrm{R}\right)$	24
3R2P	R_{sa}	$\mathrm{PP}\hat{\mathrm{R}}\hat{\mathrm{R}}$	$(R_{1sa}\mathrm{PP})\hat{\mathrm{R}}_1\hat{\mathrm{R}}$	3
		$\left(\left(\overline{\mathrm{P}}\tilde{\mathrm{P}}\mathrm{R}_1\right)\mathrm{R}\right)$	$\left(\left(\overline{\mathrm{P}}\tilde{\mathrm{P}}\mathrm{R}_1\right)(\mathrm{R}_2\mathrm{R}_{2sa})\right)$	12
	P_{sa}	$\left(\left(\overline{\mathrm{P}}\mathrm{R}_1\mathrm{R}_1\right)\mathrm{R}\right)$	$\left(\left(\dot{\mathrm{P}}_{sa}\overline{\mathrm{P}}\mathrm{R}_1\mathrm{R}_1\right)\mathrm{R}\right)$	24
4R1P	R_{sa}	$\left(\left(\overline{\mathrm{P}}R_1R_1\right)R\right)$	$\left(\left(\overline{\mathrm{P}}R_1R_1\right)(R_2R_{2sa})\right)$	12
	P_{sa}	$((\mathrm{R}_1\mathrm{R}_1\mathrm{R}_1)\mathrm{R})$	$\left(\left(\dot{\mathrm{P}}_{sa}\mathrm{R}_1\mathrm{R}_1\mathrm{R}_1\right)\mathrm{R}\right)$	8
5R	R_{sa}	$((\mathrm{R}_1\mathrm{R}_1\mathrm{R}_1)\mathrm{R})$	$((\mathrm{R}_1\mathrm{R}_1\mathrm{R}_1)(\mathrm{R}_2\mathrm{R}_{2sa}))$	4

Note: (i) $\mathrm{R}_2\mathrm{R}_2$ indicates that the axes of the revolute pairs were parallel, (ii) $\dot{\mathrm{P}}$ indicates that the axis of the prismatic pair was not perpendicular to that of the revolute pair R_1, (iii) Points (i) and (ii) are equally valid in the following

Based on Eqs. (18) and (20), the twist system of main active and passive kinematic pairs can be expressed as:

$$\begin{cases} \$_{i1} = \left(1\ 0\ 0\ ;\ 0\ 0\ 0\right), \\ \$_{i3} = \left(-Q_{ri1}\ P_{ri1}\ 0\ ;\ 0\ 0\ 0\right), \\ \$_{i4} = \left(-R_{ri1}\ 0\ P_{ri1}\ ;\ 0\ 0\ 0\right), \\ \$_{i5} = \left(0\ 0\ 0\ ;\ -M_{ri2}\ L_{ri2}\ 0\right), \\ \$_{i6} = \left(0\ 0\ 0\ ;\ -N_{ri2}\ 0\ L_{ri2}\right). \end{cases} \tag{22}$$

Other forms of twisting were obtained using a linear combination of the five twists in Eq. (22). However, the twists after the linear combination must be linearly independent. The case of redundant kinematics in the limb was not considered. That is, only the case where the connectivity of the main active and passive kinematic pairs was five was considered. The kinematic pair structures from the obtained twist system whose passive kinematic pairs were according to those listed in Table 1 were selected, as listed in Table 3.

The following conditions must be satisfied for the structure of the main active and passive kinematic pairs, as listed in Table 3:

(i) The revolute pair must be divided into two groups, the axis of the first group must intersect the rotation center of the moving platform, the axis of the second group must be parallel to each other, and all revolute pairs must belong to one of the two groups.
(ii) The number of revolute pairs belonging to the same group must be less than four.
(iii) The number of revolute pairs belonging to the first group must be greater than one.
(iv) When two revolute pairs belong to the first group, the axis of the prismatic pair must be perpendicular to that of the revolute pair belonging to the second group.
(v) The number of prismatic pairs must be less than three.

4.4 Type Synthesis of the PSAARR

The kinematic pair structures in accordance with those listed in Table 2 and Table 3 were selected based on the determination of the passive and active kinematic pair structures, which was the limb structure of the PSAARR. The case of redundant kinematics in the limb was not considered. That is, only the case where the connectivity of the limb kinematic pairs was six was considered. The limb structure of the PSAARR is listed in Table 4 and a portion of the limb structure model is shown in Figure 3.

As shown in Table 4, 93 types of PSAARR limb structures were obtained. A PSAARR was obtained by arbitrarily selecting three limb structures from the type synthesis results in Table 4 and connecting them to the moving and static platforms. This was done because the six-DOF limbs did not constrain the moving platform.

The 3 - $\mathrm{R}_{1\mathrm{ma}}\overline{\mathrm{P}}\tilde{\mathrm{P}}\dot{\mathrm{P}}_{\mathrm{sa}}\hat{\mathrm{R}}\hat{\mathrm{R}}$ PSAARR belonging to category 3R3P is shown in Figure 4. For each limb: The first kinematic pair (revolute pair) is perpendicular to the second and third kinematic pairs (prismatic pairs), and not perpendicular to the fourth kinematic pair (prismatic pair); the two revolute pairs closest to the moving platform intersect the rotation center of the moving platform.

The 3 - $\mathrm{R}_{1\mathrm{ma}}\overline{\mathrm{P}}\tilde{\mathrm{P}}\mathrm{R}_{2\mathrm{sa}}\hat{\mathrm{R}}_2\hat{\mathrm{R}}$ PSAARR belonging to category 4R2P is shown in Figure 5. For each limb: The first kinematic pair (revolute pair) is perpendicular to the second and third kinematic pairs (prismatic pairs); the fourth kinematic pair (revolute pair) and the fifth kinematic pair (revolute pair) are parallel to each other; the two revolute pairs closest to the moving platform intersect the rotation center of the moving platform.

The 3 - $\mathrm{R}_1\mathrm{R}_1\mathrm{R}_1\dot{\mathrm{P}}_{\mathrm{sa}}\hat{\mathrm{R}}_{\mathrm{ma}}\hat{\mathrm{R}}$ PSAARR belonging to category 5R1P is shown in Figure 6. For each limb: The three kinematic pairs closest to the static platform are parallel to each other, and not perpendicular to the fourth kinematic pair (prismatic pair); the two revolute pairs closest to the moving platform intersect the rotation center of the moving platform.

Table 3 Main active and passive kinematic pairs of PSAARR

Category	Main active kinematic pair	Passive kinematic pair	Type	Quantity
3R2P	R_{ma}	$\mathrm{PP}\hat{\mathrm{R}}\hat{\mathrm{R}}$	$\left(\mathrm{R}_{1\mathrm{ma}}\overline{\mathrm{P}}\tilde{\mathrm{P}}\right)\hat{\mathrm{R}}\hat{\mathrm{R}}$ $\mathrm{PP}\left(\hat{\mathrm{R}}\hat{\mathrm{R}}\hat{\mathrm{R}}_{\mathrm{ma}}\right)$	6
		$\left(\left(\overline{\mathrm{P}}\tilde{\mathrm{P}}\mathrm{R}_1\right)\mathrm{R}\right)$	$\left(\overline{\mathrm{P}}\tilde{\mathrm{P}}\mathrm{R}_1\right)\left(\hat{\mathrm{R}}\hat{\mathrm{R}}_{\mathrm{ma}}\right)$	6
4R1P	R_{ma}	$\left(\left(\overline{\mathrm{P}}\mathrm{R}_1\mathrm{R}_1\right)\mathrm{R}\right)$	$\left(\overline{\mathrm{P}}\mathrm{R}_1\mathrm{R}_1\right)\left(\hat{\mathrm{R}}\hat{\mathrm{R}}_{\mathrm{ma}}\right)$	6
5R	R_{ma}	$\left(\left(\mathrm{R}_1\mathrm{R}_1\mathrm{R}_1\right)\mathrm{R}\right)$	$\mathrm{R}_1\mathrm{R}_1\mathrm{R}_1\left(\hat{\mathrm{R}}\hat{\mathrm{R}}_{\mathrm{ma}}\right)$	2

Table 4 Limb kinematic pairs of PSAARR

Category	Main active kinematic pair	Subactive	Passive kinematic pair	Type	Quantity	Example-type	Example-model
3R3P	R_{ma}	P_{sa}	$PP\hat{R}\hat{R}$	$\left(R_{1ma}\dot{P}_{sa}\overline{P}\tilde{P}\right)\hat{R}\hat{R}$	12	$R_{1ma}\overline{P}\tilde{P}\dot{P}_{sa}\hat{R}\hat{R}$	Figure 3(a)
				$(P_{sa}PP)\left(\hat{R}\hat{R}\hat{R}_{ma}\right)$	9	$PPP_{sa}\hat{R}_{ma}\hat{R}\hat{R}$	Figure 3(b)
			$\left(\left(\overline{P}\tilde{P}R_1\right)R\right)$	$\left(\dot{P}_{sa}\overline{P}\tilde{P}R_1\right)\left(\hat{R}\hat{R}_{ma}\right)$	24	$\overline{P}\tilde{P}R_1\dot{P}_{sa}\hat{R}_{ma}\hat{R}$	Figure 3(c)
4R2P	R_{ma}	R_{sa}	$PP\hat{R}\hat{R}$	$\left(R_{1ma}\overline{P}\tilde{P}\right)R_{2sa}\hat{R}_2\hat{R}$	3	$R_{1ma}\overline{P}\tilde{P}R_{2sa}\hat{R}_2\hat{R}$	Figure 3(d)
				$(R_{1sa}PP)\hat{R}_1\left(\hat{R}\hat{R}_{ma}\right)$	6	$PPR_{1sa}\hat{R}_1\hat{R}_{ma}\hat{R}$	Figure 3(e)
			$\left(\left(\overline{P}\tilde{P}R_1\right)R\right)$	$\left(\overline{P}\tilde{P}R_1\right)R_{2sa}\hat{R}_2\hat{R}_{ma}$	3	$\overline{P}\tilde{P}R_1R_{2sa}\hat{R}_2\hat{R}_{ma}$	Figure 3(f)
		P_{sa}	$\left(\left(\overline{P}R_1R_1\right)R\right)$	$\left(\dot{P}_{sa}\overline{P}R_1R_1\right)\left(\hat{R}\hat{R}_{ma}\right)$	24	$\overline{P}R_1R_1\dot{P}_{sa}\hat{R}_{ma}\hat{R}$	Figure 3(g)
5R1P	R_{ma}	R_{sa}	$\left(\left(\overline{P}R_1R_1\right)R\right)$	$\left(\overline{P}R_1R_1\right)R_{2sa}\hat{R}_2\hat{R}_{ma}$	3	$\overline{P}R_1R_1R_{2sa}\hat{R}_2\hat{R}_{ma}$	Figure 3(h)
		P_{sa}	$((R_1R_1R_1)R)$	$\left(\dot{P}_{sa}R_1R_1R_1\right)\left(\hat{R}\hat{R}_{ma}\right)$	8	$R_1R_1R_1\dot{P}_{sa}\hat{R}_{ma}\hat{R}$	Figure 3(i)
6R	R_{ma}	R_{sa}	$((R_1R_1R_1)R)$	$R_1R_1R_1R_{2sa}\hat{R}_2\hat{R}_{ma}$	1	$R_1R_1R_1R_{2sa}\hat{R}_2\hat{R}_{ma}$	Figure 3(j)

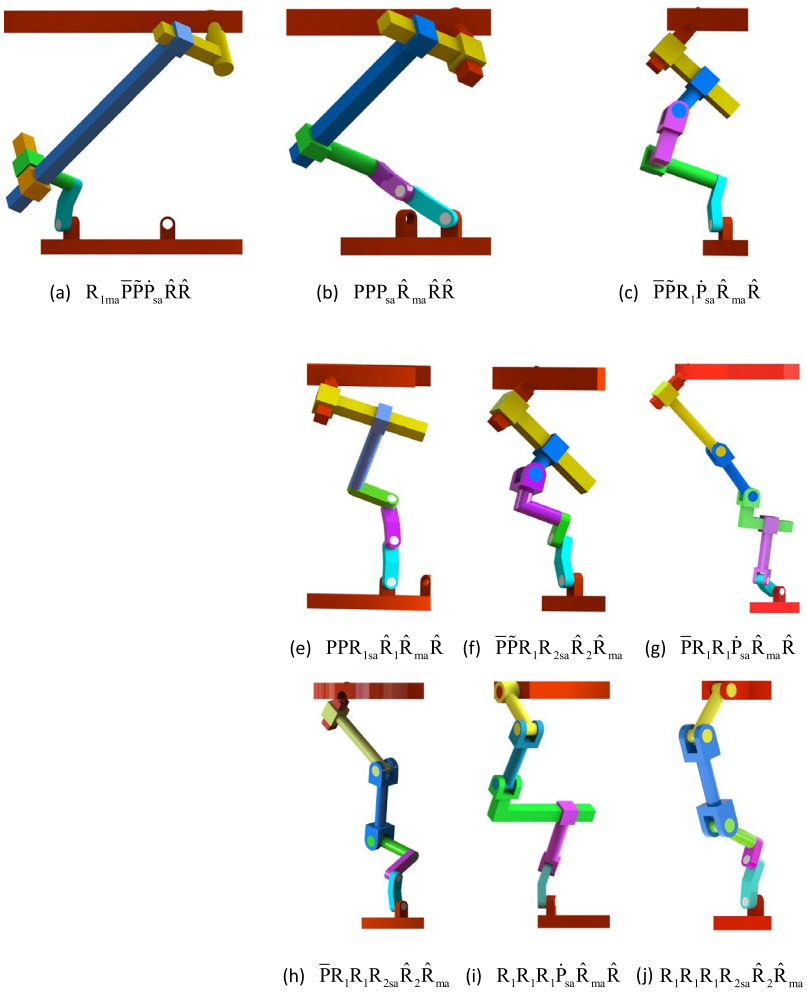

Figure 3 Limb structures of the PSAARR

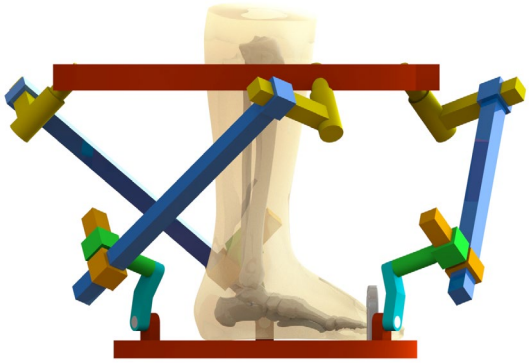

Figure 4 3—$R_{1ma}\overline{P}\tilde{P}\dot{P}_{sa}\hat{R}\hat{R}$ (3R3P) SPSAARR

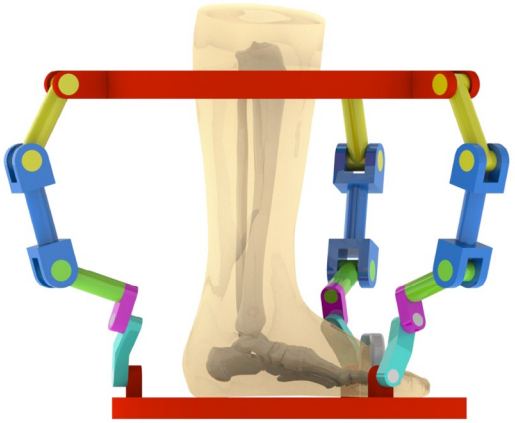

Figure 7 3 - $R_1R_1R_1R_{2sa}\hat{R}_2\hat{R}_{ma}$ (6R) PSAARR

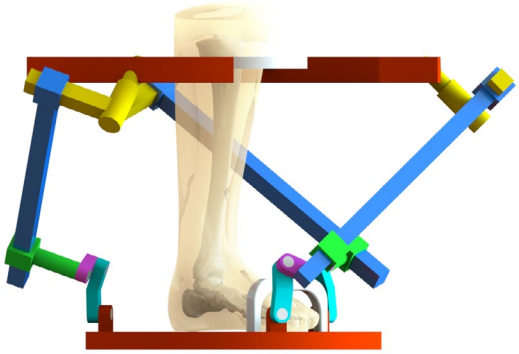

Figure 5 3 - $R_{1ma}\overline{P}\tilde{P}R_{2sa}\hat{R}_2\hat{R}$ (4R2P) PSAARR

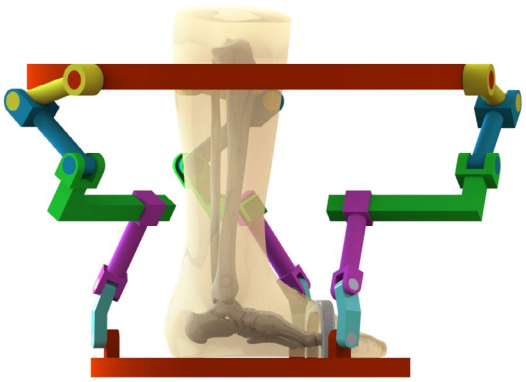

Figure 6 3 - $R_1R_1R_1\dot{P}_{sa}\hat{R}_{ma}\hat{R}$ (5R1P) PSAARR

The 3 - $R_1R_1R_1R_{2sa}\hat{R}_2\hat{R}_{ma}$ PSAARR belonging to category 6R is shown in Figure 7. For each limb: The three kinematic pairs closest to the static platform are parallel to each other; the fourth kinematic pair (revolute pair) and the fifth kinematic pair (revolute pair) are parallel to each other; the two revolute pairs closest to the moving platform intersect the rotation center of the moving platform.

The main active kinematic pair should be a frame pair to improve the performance of the robot. The subactive kinematic pair is controlled by the human body. Therefore, it should be as close as possible to the moving platform. As shown in Table 4, the two-limb structures $R_{1ma}\overline{P}\tilde{P}\dot{P}_{sa}\hat{R}\hat{R}$ and $R_{1ma}\overline{P}\tilde{P}R_{2sa}\hat{R}_2\hat{R}$ satisfied this requirement. In comparison, $R_{1ma}\overline{P}\tilde{P}\dot{P}_{sa}\hat{R}\hat{R}$ structure was simpler. Therefore, the 3 - $R_{1ma}\overline{P}\tilde{P}\dot{P}_{sa}\hat{R}\hat{R}$ symmetric parallel robot was selected as the main structure of the PSAARR.

5 Self-Alignment Capability Analysis of the PSAARR

5.1 Description of HRCC Structure

The *x*-, *y*-, and *z*-axes of the static platform coordinate system *O*-*xyz* for the rehabilitation robot coincided with the main active kinematic pair axes of the first, second, and third limbs, respectively. In addition, the origin *O* was the intersection point of the three axes. The origin *O'* of the moving platform coordinate system *O'*-*x'y'z'* was the intersection point of the axis of the revolute pair directly connected to the moving platform. The *z'*-axis pointed from point *O'* to the form center *C* of the moving platform. The *y'*-axis was located on the plane $O'CO_{16}$, which was opposite to the direction of the vector $O'O_{16}$. The *x'*-axis was determined by the right-hand rule, as shown in Figure 8.

The local coordinate system defined for each kinematic pair of the second and third limbs was the same as that of the first limb owing to the symmetrical structure. Therefore, the local coordinate system of each kinematic pair was defined considering the first limb as an example. In addition, the coordinate origin

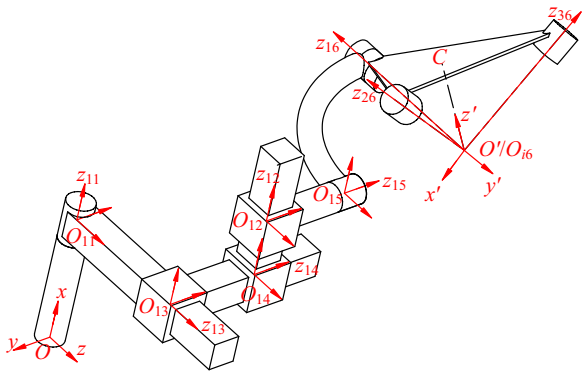

Figure 8 Local coordinate system of the first limb for each kinematic pair

O_{ij} coincided with the center point of each kinematic pair, as shown in Figure 8. The local coordinate systems O_{i5}-$x_{i5}y_{i5}z_{i5}$ and O_{i6}-$x_{i6}y_{i6}z_{i6}$ were established at the kinematic pairs O_{i5} and O_{i6}, respectively. Points O_{i5} and O_{i6} coincided with point O', and O_{i5} and O_{i6} were drawn at the kinematic pair for convenience. Simultaneously, only the z_{ij}-axis was marked to express the local coordinate system, and the x_{ij}- and y_{ij}-axes were determined according to the principle of coordinate system establishment. The axes of each kinematic pair coincided with their corresponding local coordinate systems, which is expressed as:

$$\begin{cases} {}^{O_{ij}}\hat{\boldsymbol{\omega}}_{ij} = \begin{pmatrix} 0 & 0 & 1 \end{pmatrix}^{\mathrm{T}} & (i = 1,\ 2,\ 3;\ j = 1,\ 5,\ 6), \\ {}^{O_{ij}}\hat{\boldsymbol{v}}_{ij} = \begin{pmatrix} 0 & 0 & 1 \end{pmatrix}^{\mathrm{T}} & (i = 1,\ 2,\ 3;\ j = 2,\ 3,\ 4). \end{cases} \tag{23}$$

The structural parameters of the limb are as follows: the distances between points O and O_{i1}, O_{i1} and O_{i3}, O_{i3} and O_{i4}, and O_{i4} and O_{i2} are L_1, L_2, L_3, and L_4 at the initial position, respectively. The distance between point O' and O_{i6} is L_5. The side length of equilateral triangle $O_{16}O_{26}O_{36}$ is L_6, the angle between kinematic pairs O_{i3} and O_{i4} is α, the angle between kinematic pairs O_{i5} and O_{i6} is β, and the angle between axes $O_{i6}O$ and OC is γ. The homogeneous transformation matrixes of each adjacent kinematic pair for the initial pose are presented in the Appendix.

A static coordinate system was established for the human body kinematic chain at the fixed connection part between the PSAARR and human lower leg, which coincided with the static platform coordinate system of the PSAARR. In addition, a moving coordinate system was established at the center of the human talus, which coincided with the moving platform coordinate system of the PSAARR. The homogeneous transformation matrix of the moving coordinate system O'-$x'y'z'$ with respect to the static coordinate system O-xyz is expressed as:

$${}^{O}_{O'}\boldsymbol{T}(\boldsymbol{q}) = \begin{pmatrix} {}^{O}_{O'}\boldsymbol{R} & {}^{O}\boldsymbol{p}_{O'} \\ \boldsymbol{0} & 1 \end{pmatrix} = \begin{pmatrix} r_{11} & r_{12} & r_{13} & p_x \\ r_{21} & r_{22} & r_{23} & p_y \\ r_{31} & r_{32} & r_{33} & p_z \\ 0 & 0 & 0 & 1 \end{pmatrix}, \tag{24}$$

where $(r_{11},\ r_{21},\ r_{31})^{\mathrm{T}}$, $(r_{12},\ r_{22},\ r_{32})^{\mathrm{T}}$, and $(r_{13},\ r_{23},\ r_{33})^{\mathrm{T}}$ represent the direction vectors of the x'-, y'-, and z'-axes, respectively. Additionally, r_{ij} $(i = 1, 2, 3;\ j = 1, 2, 3)$ denotes known numbers when the rehabilitation locomotion mode is given. $(p_x,\ p_y,\ p_z)^{\mathrm{T}}$ represents the position vector of point O', and p_x, p_y, and p_z are known numbers according to the position of the human talus center.

There are two paths from the origin O of the static coordinate system O-xyz to the origin O' of the moving coordinate system O'-$x'y'z'$ for the HRCC of the PSAARR, that is, the PSAARR and human body. Subsequently, the homogeneous transformation matrix between the two coordinate systems of the human body path is known. Therefore, all displacement or rotation angles of the PSAARR active kinematic pair can be obtained according to the kinematic constraint equation of the HRCC.

From the previous analysis, the position and orientation of the PSAARR moving platform were decoupled, such that they could be calculated from the human talar center position and rehabilitation locomotion mode, respectively.

5.2 Kinematic Position Analysis of the HRCC

From the previous analysis, point O_{i5} coincided with point O', that is, ${}^{O}p_{O'} = {}^{O}p_{Oi5.}$ Therefore, it was only necessary to know the homogeneous transformation matrix ${}^{O}_{O_{i5}}\boldsymbol{T}(\boldsymbol{q})$ (the coordinate system O_{i5}-$x_{i5}y_{i5}z_{i5}$ with respect to the static platform coordinate system O-xyz) to obtain ${}^{O}p_{O'}$.

According to the exponential product equation, ${}^{O}_{O_{i5}}\boldsymbol{T}(\boldsymbol{q})$ can be expressed as:

$${}^{O}_{O_{i5}}\boldsymbol{T}(\boldsymbol{q}) = e^{\theta_{i1}\left[{}^{O}\hat{\$}_{i1}\right]} e^{d_{i3}\left[{}^{O}\hat{\$}_{i3}\right]} e^{d_{i4}\left[{}^{O}\hat{\$}_{i4}\right]} e^{d_{i2}\left[{}^{O}\hat{\$}_{i2}\right]} {}^{O}_{O_{i5}}\boldsymbol{T}(\boldsymbol{0}), \tag{25}$$

where θ_{i1} represents the rotation angle of the main active kinematic pair in the ith limb, d_{ij} $(j = 2, 3, 4)$ represents the displacement of the jth prismatic pair in the ith limb, and ${}^{O}\hat{\$}_{ij}$ represents the unit twist of the jth kinematic pair relative to the static platform coordinate system O-xyz

when all kinematic pairs of the *i*th limb (except the *j*th kinematic pair) are fixed in the initial configuration.

For the first limb, the unit twist ${}^{O}\hat{\$}_{ij}$ is expressed as:

$$\begin{cases} {}^{O}\hat{\$}_{11}=(1\ 0\ 0\ ;\ 0\ 0\ 0), \\ {}^{O}\hat{\$}_{13}=(0\ 0\ 0\ ;\ 0\ 0\ 1), \\ {}^{O}\hat{\$}_{14}=(0\ 0\ 0\ ;\ 0\ -s\alpha\ \ c\alpha), \\ {}^{O}\hat{\$}_{12}=(0\ 0\ 0\ ;\ 1\ 0\ 0). \end{cases} \tag{26}$$

where $s\alpha$ represents $\sin\alpha$ and $c\alpha$ represents $\cos\alpha$.

For the second limb, the unit twist ${}^{O}\hat{\$}_{ij}$ is expressed as:

$$\begin{cases} {}^{O}\hat{\$}_{21}=(0\ 1\ 0\ ;\ 0\ 0\ 0), \\ {}^{O}\hat{\$}_{23}=(0\ 0\ 0\ ;\ 1\ 0\ 0), \\ {}^{O}\hat{\$}_{24}=(0\ 0\ 0\ ;\ c\alpha\ \ 0\ \ -s\alpha), \\ {}^{O}\hat{\$}_{22}=(0\ 0\ 0\ ;\ 0\ 1\ 0). \end{cases} \tag{27}$$

For the third limb, the unit twist ${}^{O}\hat{\$}_{ij}$ is expressed as:

$$\begin{cases} {}^{O}\hat{\$}_{31}=(0\ 0\ 1\ ;\ 0\ 0\ 0), \\ {}^{O}\hat{\$}_{33}=(0\ 0\ 0\ ;\ 0\ 1\ 0), \\ {}^{O}\hat{\$}_{34}=(0\ 0\ 0\ ;\ -s\alpha\ \ c\alpha\ \ 0), \\ {}^{O}\hat{\$}_{32}=(0\ 0\ 0\ ;\ 0\ 0\ 1). \end{cases} \tag{28}$$

For the revolute pair, the exponential product is expressed as:

$$\begin{cases} \hat{\$}_{ij}=\begin{pmatrix}\hat{\boldsymbol{\omega}}_{ij}\\ \boldsymbol{v}_{ij}\end{pmatrix}=\begin{pmatrix}\hat{\boldsymbol{\omega}}_{ij}\\ \boldsymbol{r}_{ij}\times\hat{\boldsymbol{\omega}}_{ij}\end{pmatrix}\quad(\boldsymbol{\omega}_{ij}\neq\boldsymbol{0}), \\ e^{\theta_{ij}\left[\hat{\$}_{ij}\right]}=\begin{pmatrix}e^{\theta_{ij}[\hat{\boldsymbol{\omega}}_{ij}]} & \left(\boldsymbol{E}-e^{\theta_{ij}[\hat{\boldsymbol{\omega}}_{ij}]}\right)(\hat{\boldsymbol{\omega}}_{ij}\times\boldsymbol{v}_{ij})+\theta_{ij}\hat{\boldsymbol{\omega}}_{ij}\hat{\boldsymbol{\omega}}_{ij}^{\mathrm{T}}\boldsymbol{v}_{ij}\\ \boldsymbol{0} & 1\end{pmatrix}. \end{cases} \tag{29}$$

The exponential product for the prismatic pair is expressed as:

$$\hat{\$}_{ij}=\begin{pmatrix}\boldsymbol{0}\\ \hat{\boldsymbol{v}}_{ij}\end{pmatrix},\ e^{d_{ij}\left[\hat{\$}_{ij}\right]}=\begin{pmatrix}\boldsymbol{E} & d_{ij}\hat{\boldsymbol{v}}_{ij}\\ \boldsymbol{0} & 1\end{pmatrix}, \tag{30}$$

where $\hat{\boldsymbol{\omega}}_{ij}$ represents the unit vector of the *j*th revolute pair axis direction in the *i*th limb, r_{ij} represents any point vector diameter of the *j*th revolute pair axis in the *i*th limb, $\hat{\boldsymbol{v}}_{ij}$ represents the unit vector of the *j*th prismatic pair axis in the *i*th limb, and $\left[\hat{\boldsymbol{\omega}}_{ij}\right]$ represents the antisymmetric matrix of $\hat{\boldsymbol{\omega}}_{ij}$.

According to the homogeneous transformation rule, ${}^{O}_{O_{i5}}\boldsymbol{T}(\boldsymbol{0})$ can be expressed as:

$${}^{O}_{O_{i5}}\boldsymbol{T}(\boldsymbol{0})={}^{O}_{O_{i1}}\boldsymbol{T}(\boldsymbol{0})\,{}^{O_{i1}}_{O_{i3}}\boldsymbol{T}(\boldsymbol{0})\,{}^{O_{i3}}_{O_{i4}}\boldsymbol{T}(\boldsymbol{0})\,{}^{O_{i4}}_{O_{i2}}\boldsymbol{T}(\boldsymbol{0})\,{}^{O_{i2}}_{O_{i5}}\boldsymbol{T}(\boldsymbol{0}). \tag{31}$$

Combining Eqs. (25)–(31) results in:

$$\begin{aligned} {}^{O}\boldsymbol{p}_{O'}&=\begin{pmatrix}I_1\\ f_{12}(d_{13},\ d_{14})\\ f_{13}(d_{13},\ d_{14})\end{pmatrix}=\begin{pmatrix}f_{21}(d_{23},\ d_{24})\\ I_2\\ f_{23}(d_{23},\ d_{24})\end{pmatrix}\\ &=\begin{pmatrix}f_{31}(d_{33},\ d_{34})\\ f_{32}(d_{33},\ d_{34})\\ I_3\end{pmatrix}, \end{aligned} \tag{32}$$

where $I_1=d_{12}+p_{45z}+(L_1+L_4)$, $I_2=d_{22}+p_{45z}+(L_1+L_4)$, and $I_3=d_{32}+p_{45z}+(L_1+L_4)$.

Combining Eqs. (24)–(32) results in:

$$\begin{cases} d_{12}=p_x-p_{45z}-(L_1+L_4), \\ d_{22}=p_y-p_{45z}-(L_1+L_4), \\ d_{32}=p_z-p_{45z}-(L_1+L_4). \end{cases} \tag{33}$$

The central position of the talus was only related to the position of the subactive kinematic pair, not the main active kinematic pair, as seen in Eq. (33). Moreover, the different directional positions of the talus were only related to the position of the limb subactive kinematic pair. Therefore, the moving platform positions were completely decoupled.

5.3 Kinematic Orientation Analysis of the HRCC

According to the included angle between the kinematic pair, the O_{i5} and O_{i6} axis is β, and the relationship between ${}^{O}\hat{\boldsymbol{\omega}}_{i5}$, ${}^{O}\hat{\boldsymbol{\omega}}_{i6}$, and β is expressed as:

$${}^{O}\hat{\boldsymbol{\omega}}_{i5}\cdot{}^{O}\hat{\boldsymbol{\omega}}_{i6}=\cos\beta. \tag{34}$$

Using homogeneous transformation, the homogeneous coordinates of ${}^{O}\hat{\boldsymbol{\omega}}_{i5}$ and ${}^{O}\hat{\boldsymbol{\omega}}_{i6}$ is expressed as:

$$\begin{cases} \begin{pmatrix}{}^{O}\hat{\boldsymbol{\omega}}_{i5}\\ 0\end{pmatrix}={}^{O}_{O_{i5}}\boldsymbol{T}(\boldsymbol{q})\begin{pmatrix}{}^{O_{i5}}\hat{\boldsymbol{\omega}}_{i5}\\ 0\end{pmatrix}, \\ \begin{pmatrix}{}^{O}\hat{\boldsymbol{\omega}}_{i6}\\ 0\end{pmatrix}={}^{O}_{O'}\boldsymbol{T}(\boldsymbol{q})\,{}^{O'}_{O_{i6}}\boldsymbol{T}(\boldsymbol{q})\begin{pmatrix}{}^{O_{i6}}\hat{\boldsymbol{\omega}}_{i6}\\ 0\end{pmatrix}. \end{cases} \tag{35}$$

Combining Eqs. (25) and (35) results in:

$$\begin{cases} {}^{O}\hat{\boldsymbol{\omega}}_{15} = \begin{pmatrix} a_{33} \\ -a_{13}\mathrm{s}\theta_{11} - a_{23}\mathrm{c}\theta_{11} \\ a_{13}\mathrm{c}\theta_{11} - a_{23}\mathrm{s}\theta_{11} \end{pmatrix}, \\ {}^{O}\hat{\boldsymbol{\omega}}_{25} = \begin{pmatrix} a_{13}\mathrm{c}\theta_{21} - a_{23}\mathrm{s}\theta_{21} \\ a_{33} \\ -a_{13}\mathrm{s}\theta_{21} - a_{23}\mathrm{c}\theta_{21} \end{pmatrix}, \\ {}^{O}\hat{\boldsymbol{\omega}}_{35} = \begin{pmatrix} -a_{13}\mathrm{s}\theta_{31} - a_{23}\mathrm{c}\theta_{31} \\ a_{13}\mathrm{c}\theta_{31} - a_{23}\mathrm{s}\theta_{31} \\ a_{33} \end{pmatrix}. \end{cases} \tag{36}$$

According to the exponential product formula, ${}^{O'}_{O_{i6}}\boldsymbol{T}(\boldsymbol{q})$ can be expressed as:

$${}^{O'}_{O_{i6}}\boldsymbol{T}(\boldsymbol{q}) = e^{\theta_{i6}\left[{}^{O'}\hat{\$}_{i6}\right]}{}^{O'}_{O_{i6}}\boldsymbol{T}(\boldsymbol{0}). \tag{37}$$

According to the positional relationship between the kinematic pair, the twist ${}^{O'}\hat{\$}_{i6}$ can be expressed as:

$$\begin{cases} {}^{O'}\hat{\$}_{26} = \left(0 \ -\mathrm{s}\gamma \ \ \mathrm{c}\gamma \ ; \ 0 \ 0 \ 0\right), \\ {}^{O'}\hat{\$}_{26} = \left(\left(\sqrt{3}\mathrm{s}\gamma\right)\Big/2 \ (\mathrm{s}\gamma)/2 \ \ \mathrm{c}\gamma \ ; \ 0 \ 0 \ 0\right), \\ {}^{O'}\hat{\$}_{36} = \left(-\left(\sqrt{3}\mathrm{s}\gamma\right)\Big/2 \ (\mathrm{s}\gamma)/2 \ \ \mathrm{c}\gamma \ ; \ 0 \ 0 \ 0\right). \end{cases} \tag{38}$$

Combining Eqs. (35), (37), and (38) results in:

$$\begin{cases} {}^{O}\hat{\boldsymbol{\omega}}_{16} = \begin{pmatrix} r_{13}c\gamma - r_{12}s\gamma \\ r_{23}c\gamma - r_{22}s\gamma \\ r_{33}c\gamma - r_{32}s\gamma \end{pmatrix} = \begin{pmatrix} A_{11} \\ A_{12} \\ A_{13} \end{pmatrix}, \\ {}^{O}\hat{\boldsymbol{\omega}}_{26} = \begin{pmatrix} \left(\sqrt{3}r_{11}s\gamma\right)\Big/2 + (r_{12}s\gamma)/2 + r_{13}c\gamma \\ \left(\sqrt{3}r_{21}s\gamma\right)\Big/2 + (r_{22}s\gamma)/2 + r_{23}c\gamma \\ \left(\sqrt{3}r_{31}s\gamma\right)\Big/2 + (r_{32}s\gamma)/2 + r_{33}c\gamma \end{pmatrix} = \begin{pmatrix} A_{21} \\ A_{22} \\ A_{23} \end{pmatrix}, \\ {}^{O}\hat{\boldsymbol{\omega}}_{36} = \begin{pmatrix} (r_{12}s\gamma)/2 + r_{13}c\gamma - \left(\sqrt{3}r_{11}s\gamma\right)\Big/2 \\ (r_{22}s\gamma)/2 + r_{23}c\gamma - \left(\sqrt{3}r_{21}s\gamma\right)\Big/2 \\ (r_{32}s\gamma)/2 + r_{33}c\gamma - \left(\sqrt{3}r_{31}s\gamma\right)\Big/2 \end{pmatrix} = \begin{pmatrix} A_{31} \\ A_{32} \\ A_{33} \end{pmatrix}. \end{cases} \tag{39}$$

Combining Eqs. (34), (36) and (39) results in:

$$B_{i1}\mathrm{s}\theta_{i1} + B_{i2}\mathrm{c}\theta_{i1} + B_{i3} = 0 \quad (i = 1,\ 2,\ 3), \tag{40}$$

$$\begin{cases} B_{11} = -a_{13}A_{12} - a_{23}A_{13}, \\ B_{12} = a_{13}A_{13} - a_{23}A_{12}, \\ B_{13} = a_{33}A_{11} - \cos\beta, \end{cases} \quad \begin{cases} B_{21} = -a_{13}A_{23} - a_{23}A_{21}, \\ B_{22} = a_{13}A_{21} - a_{23}A_{23}, \\ B_{23} = a_{33}A_{22} - \cos\beta, \end{cases} \quad \begin{cases} B_{31} = -a_{13}A_{31} - a_{23}A_{32}, \\ B_{32} = a_{13}A_{32} - a_{23}A_{31}, \\ B_{33} = a_{33}A_{33} - \cos\beta. \end{cases}$$

According to Eq. (40), the rotational angle of the main active kinematic pair can be expressed as:

$$\theta_{i1} = 2a\tan\frac{B_{i1} \pm \sqrt{B_{i1}^2 + B_{i2}^2 - B_{i3}^2}}{B_{i2} - B_{i3}}. \tag{41}$$

The rehabilitation locomotion mode was only related to the rotational angle of the main active kinematic pair and not to the subactive kinematic pair, as seen in Eq. (41).

According to the inverse kinematics of position and orientation, the rehabilitation locomotion mode was only related to the rotation angle of the main active kinematic pair, and the central position of the talus was only related to the displacement of the subactive kinematic pair. Therefore, the 3-$\mathrm{R}_{1\mathrm{ma}}\overline{\mathrm{P}}\tilde{\mathrm{P}}\dot{\mathrm{P}}_{\mathrm{sa}}\hat{\mathrm{R}}\hat{\mathrm{R}}$ parallel mechanism met the requirements of the PSAARR, and the kinematic analysis results provided a theoretical basis for subsequent design, analysis, and optimization.

6 Conclusions

(1) A self-alignment principle of parallel ARR was proposed according to the conditions of "suitable passive DOF", "decoupled", and "less limb": (i) Three "suitable passive DOF" of translation were introduced on the basis of three active DOF of rotation to transform the HRCC formed by the ARR and

human body into a kinematic suitable constrained system and (ii) the active and passive DOF were decoupled, and the number of limbs was equal to the number of active DOF.

(2) The type synthesis condition was obtained according to the self-alignment principle of the PSAARR. The reciprocal product of the actuation wrench and all other twists in the same limb was zero, except for the corresponding twist. The type synthesis method of the PSAARR limb was proposed based on the screw theory and type synthesis conditions, obtaining 93 types of PSAARR limb structures.

(3) A 3-$\mathrm{R}_{1\mathrm{ma}}\overline{\mathrm{P}}\tilde{\mathrm{P}}\dot{\mathrm{P}}_{\mathrm{sa}}\hat{\mathrm{R}}\hat{\mathrm{R}}$ symmetric parallel robot was selected as the main structure of the PSAARR. The results of the kinematic analysis showed that the rotational angle of the main active kinematic pair was only related to the rehabilitation locomotion mode and the displacement of the subactive kinematic pair was only related to the central position of the talus, which met the requirements of the PSAARR.

Appendix

$$ {}^{O}_{O_{11}}\boldsymbol{T}(\mathbf{0})=\begin{pmatrix} 0 & 0 & 1 & L_1 \\ 0 & -1 & 0 & 0 \\ 1 & 0 & 0 & 0 \\ 0 & 0 & 0 & 1 \end{pmatrix}, \tag{A1} $$

$$ {}^{O}_{O_{21}}\boldsymbol{T}(\mathbf{0})=\begin{pmatrix} 1 & 0 & 0 & 0 \\ 0 & 0 & 1 & L_1 \\ 0 & -1 & 0 & 0 \\ 0 & 0 & 0 & 1 \end{pmatrix}, \tag{A2} $$

$$ {}^{O}_{O_{31}}\boldsymbol{T}(\mathbf{0})=\begin{pmatrix} 0 & -1 & 0 & 0 \\ 1 & 0 & 0 & 0 \\ 0 & 0 & 1 & L_1 \\ 0 & 0 & 0 & 1 \end{pmatrix}, \tag{A3} $$

$$ {}^{O_{i1}}_{O_{i3}}\boldsymbol{T}(\mathbf{0}) = \begin{pmatrix} 0 & 0 & 1 & L_2 \\ 1 & 0 & 0 & 0 \\ 0 & 1 & 0 & 0 \\ 0 & 0 & 0 & 1 \end{pmatrix}, \tag{A4} $$

$$ {}^{O_{i3}}_{O_{i4}}\boldsymbol{T}(\mathbf{0}) = \begin{pmatrix} -\mathrm{c}\alpha & 0 & \mathrm{s}\alpha & L_3\mathrm{s}\alpha \\ 0 & -1 & 0 & 0 \\ \mathrm{s}\alpha & 0 & \mathrm{c}\alpha & L_3\mathrm{c}\alpha \\ 0 & 0 & 0 & 1 \end{pmatrix}, \tag{A5} $$

$$ {}^{O_{i4}}_{O_{i2}}\boldsymbol{T}(\mathbf{0}) = \begin{pmatrix} \mathrm{s}\alpha & -\mathrm{c}\alpha & 0 & 0 \\ 0 & 0 & -1 & -L_4 \\ \mathrm{c}\alpha & \mathrm{s}\alpha & 0 & 0 \\ 0 & 0 & 0 & 1 \end{pmatrix}, \tag{A6} $$

$$ {}^{O_{i2}}_{O_{i5}}\boldsymbol{T}(\mathbf{0}) = \begin{pmatrix} a_{11} & a_{12} & a_{13} & p_{45x} \\ a_{21} & a_{22} & a_{23} & p_{45y} \\ a_{31} & a_{32} & a_{33} & p_{45z} \\ 0 & 0 & 0 & 1 \end{pmatrix}, \tag{A7} $$

$$ {}^{O_{i5}}_{O_{i6}}\boldsymbol{T}(\mathbf{0}) = \begin{pmatrix} \mathrm{c}\beta & 0 & \mathrm{s}\beta & 0 \\ 0 & 1 & 0 & 0 \\ -\mathrm{s}\beta & 0 & \mathrm{c}\beta & 0 \\ 0 & 0 & 0 & 1 \end{pmatrix}, \tag{A8} $$

$$ {}^{O'}_{O_{16}}\boldsymbol{T}(\mathbf{0}) = \begin{pmatrix} 0 & -1 & 0 & 0 \\ \mathrm{c}\gamma & 0 & -\mathrm{s}\gamma & 0 \\ \mathrm{s}\gamma & 0 & \mathrm{c}\gamma & 0 \\ 0 & 0 & 0 & 1 \end{pmatrix}, \tag{A9} $$

$$ {}^{O'}_{O_{26}}\boldsymbol{T}(\mathbf{0}) = \begin{pmatrix} -\frac{\sqrt{3}}{2}\mathrm{c}\gamma & \frac{1}{2} & \frac{\sqrt{3}}{2}\mathrm{s}\gamma & 0 \\ -\frac{1}{2}\mathrm{c}\gamma & -\frac{\sqrt{3}}{2} & \frac{1}{2}\mathrm{s}\gamma & 0 \\ \mathrm{s}\gamma & 0 & \mathrm{c}\gamma & 0 \\ 0 & 0 & 0 & 1 \end{pmatrix}, \tag{A10} $$

$$ {}^{O'}_{O_{36}}\boldsymbol{T}(\mathbf{0}) = \begin{pmatrix} \frac{\sqrt{3}}{2}\mathrm{c}\gamma & \frac{1}{2} & -\frac{\sqrt{3}}{2}\mathrm{s}\gamma & 0 \\ -\frac{1}{2}\mathrm{c}\gamma & \frac{\sqrt{3}}{2} & \frac{1}{2}\mathrm{s}\gamma & 0 \\ \mathrm{s}\gamma & 0 & \mathrm{c}\gamma & 0 \\ 0 & 0 & 0 & 1 \end{pmatrix}. \tag{A11} $$

Acknowledgements
Not applicable.

Authors' Contributions
YL and WL wrote the manuscript; DF and WT assisted with theoretical analyses, and BH and DZ was responsible for proof reading. All authors read and approved the final manuscript.

Funding
Supported by Key Scientific Research Platforms and Projects of Guangdong Regular Institutions of Higher Education of China (Grant No. 2022KCXTD033), Guangdong Provincial Natural Science Foundation of China (Grant No. 2023A1515012103), Guangdong Provincial Scientific Research Capacity Improvement Project of Key Developing Disciplines of China (Grant No. 2021ZDJS084), National Natural Science Foundation of China (Grant No. 52105009).

Data availability
The data that support the findings of this study are available from the corresponding author upon reasonable request.

Declarations

Competing Interests
The authors declare no competing financial interests.

Received: 3 October 2022 Revised: 4 January 2024 Accepted: 12 January 2024
Published online: 06 March 2024

References

[1] F Alnajjar, R Zaier, S Khalid, et al. Trends and technologies in rehabilitation of foot drop: A systematic review. *Expert Review of Medical Devices*, 2021, 18(1): 31-46.
[2] M J Dong, Y Zhou, J F Li, et al. State of the art in parallel ankle rehabilitation robot: A systematic review. *Journal of NeuroEngineering and Rehabilitation*, 2021, 18(1): 1-15.
[3] D Shi, W X Zhang, W Zhang, et al. A review on lower limb rehabilitation exoskeleton robots. *Chinese Journal of Mechanical Engineering*, 2019, 32(1): 1-11.
[4] X B Chen, S Zhang, K B Cao, et al. Development of a wearable upper limb rehabilitation robot based on reinforced soft pneumatic actuators. *Chinese Journal of Mechanical Engineering*, 2022, 35(1): 1-9.
[5] P E Dupont, B J Nelson, M Goldfarb, et al. A decade retrospective of medical robotics research from 2010 to 2020. *Science Robotics*, 2021, 6(60): eabi8017.
[6] X F Zeng, G L Zhu, M M Zhang, et al. Reviewing clinical effectiveness of active training strategies of platform-based ankle rehabilitation robots. *Journal of Healthcare Engineering*, 2018: 2858294.
[7] S Hussain, P K Jamwal, P V Vliet, et al. Robot assisted ankle neuro-rehabilitation: state of the art and future challenges. *Expert Review of Neurotherapeutics*, 2021, 21(1): 111-121.
[8] B Shi, X F Chen, Z Yue, et al. Wearable ankle robots in post-stroke rehabilitation of gait: a systematic review. *Frontiers in Neurorobotics*, 2019, 13: 63.
[9] X Y Wang, S Guo, B J Qu, et al. Design of a passive gait-based ankle-foot exoskeleton with self-adaptive capability. *Chinese Journal of Mechanical Engineering*, 2020, 33(1): 1-11.
[10] A B Payedimarri, M Ratti, R Rescinito, et al. Effectiveness of platform-based robot-assisted rehabilitation for musculoskeletal or neurologic injuries: A systematic review. *Bioengineering*, 2022, 9(4): 129.
[11] B Hu, D S Shi, T F Xie, et al. Kinematically identical manipulators derivation for the 2-RPU+UPR parallel manipulator and their constraint performance comparison. *Journal of Mechanisms and Robotics*, 2020, 12: 061011.
[12] K J Dong, D L Li, X Y Xue, et al. Workspace and accuracy analysis on a novel 6-UCU bone-attached parallel manipulator. *Chinese Journal of Mechanical Engineering*, 2022, 35: 35.
[13] J S Dai, T S Zhao, C Nester. Sprained ankle physiotherapy based mechanism synthesis and stiffness analysis of a robotic rehabilitation device. *Autonomous Robots*, 2004, 16(2): 207-218.
[14] J A Saglia, N G Tsagarakis, J S Dai, et al. Control strategies for patient-assisted training using the ankle rehabilitation robot (ARBOT). *IEEE/ASME Transactions on Mechatronics*, 2012, 18(6): 1799-1808.
[15] Q S Ai, C X Zhu, J Zuo, et al. Disturbance-estimated adaptive backstepping sliding mode control of a pneumatic muscles-driven ankle rehabilitation robot. *Sensors*, 2017, 18(1): 66.
[16] Y H Tsoi, S Q Xie. Design and control of a parallel robot for ankle rehabilitation. *International Journal of Intelligent Systems Technologies and Applications*, 2010, 8(1-4): 100-113.
[17] Y H Tsoi, S Q Xie. Online estimation algorithm for a biaxial ankle kinematic model with configuration dependent joint axes. *Journal of Biomechanical Engineering*, 2011, 133(2): 021005-021016.
[18] P K Jamwal, S Hussain, M H Ghayesh, et al. Adaptive impedance control of parallel ankle rehabilitation robot. *Journal of Dynamic Systems, Measurement, and Control*, 2017, 139(11): 111006.
[19] P K Jamwal, S Hussain, Y H Tsoi, et al. Musculoskeletal model for path generation and modification of an ankle rehabilitation robot. *IEEE Transactions on Human-Machine Systems*, 2020, 50(5): 373-383.
[20] Y P Zou, A D Zhang, Q Zhang, et al. Design and experimental research of 3-RRS parallel ankle rehabilitation robot. *Micromachines*, 2022, 13(6): 950.
[21] M M Zhang, J H Cao, G L Zhu, et al. Reconfigurable workspace and torque capacity of a compliant ankle rehabilitation robot (CARR). *Robotics and Autonomous Systems*, 2017, 98: 213-221.
[22] K Qian, Z L Li, Z Q Zhang, et al. Data-driven adaptive iterative learning control of a compliant rehabilitation robot for repetitive ankle training. *IEEE Robotics and Automation Letters*, 2022, 8(2): 656-663.
[23] J F Li, S P Zuo, L Y Zhang, et al. Mechanical design and performance analysis of a novel parallel robot for ankle rehabilitation. *Journal of Mechanisms and Robotics*, 2020, 12(5): 051007.
[24] J F Li, W P Fan, M J Dong, et al. Implementation of passive compliance training on a parallel ankle rehabilitation robot to enhance safety. *Industrial Robot: The International Journal of Robotics Research and Applicatio*n, 2020, 47(5): 747-755.
[25] M J Dong, W P Fan, J F Li, et al. A new ankle robotic system enabling whole-stage compliance rehabilitation training. *IEEE/ASME Transactions on Mechatronics*, 2021, 26(3): 1490-1500.
[26] Q Liu, J Zuo, C X Zhu, et al. Design and hierarchical force-position control of redundant pneumatic muscles-cable-driven ankle rehabilitation robot. *IEEE Robotics and Automation Letters*, 2021, 7(1): 502-509.
[27] F J Abu-Dakka, A Valera, J A Escalera, et al. Passive exercise adaptation for ankle rehabilitation based on learning control framework. *Sensors*, 2020, 20(21): 6215.
[28] J J Zhang, C L Liu, T Liu, et al. Module combination based configuration synthesis and kinematic analysis of generalized spherical parallel mechanism for ankle rehabilitation. *Mechanism and Machine Theory*, 2021, 166: 104436.
[29] C L Liu, J J Zhang, Z H Ma, et al. Accurate detection mechanism synthesis and robot-assisted recognition method for ankle instantaneous motion. *Mechanism and Machine Theory*, 2022, 176: 105000.
[30] D X Zeng, H F Wu, X H Zhao, et al. A new type of ankle-foot rehabilitation robot based on muscle motor characteristics. *IEEE Access*, 2020, 8: 215915-215927.
[31] Y Liu, W J Lu, H F Wu, et al. Performance analysis and trajectory planning of multi-locomotion mode ankle rehabilitation robot. *Robotics and Autonomous Systems*, 2022: 104246.
[32] S Hussain, P K Jamwal, M H Ghayesh. State-of-the-art robotic devices for ankle rehabilitation: Mechanism and control review. *Proceedings of the Institution of Mechanical Engineers, Part H: Journal of Engineering in Medicine*, 2017, 231(12): 1224-1234.
[33] Y J Niu, Z B Song, J S Dai. Kinematic analysis and optimization of a planar parallel compliant mechanism for self-alignment knee exoskeleton. *Mechanical Sciences*, 2018, 9(2): 405-416.
[34] S V Sarkisian, M K Ishmael, G R Hunt, et al. Design, development, and validation of a self-aligning mechanism for high-torque powered knee exoskeletons. *IEEE Transactions on Medical Robotics and Bionics*, 2020, 2(2): 248-259.
[35] S V Sarkisian, M K Ishmael, T Lenzi. Self-aligning mechanism improves comfort and performance with a powered knee exoskeleton. *IEEE Transactions on Neural Systems and Rehabilitation Engineering*, 2021, 29: 629-640.
[36] M I Awad, I Hussain, S Ghosh, et al. A double-layered elbow exoskeleton interface with 3-PRR planar parallel mechanism for axis self-alignment. *Journal of Mechanisms and Robotics*, 2021, 13(1): 011016.
[37] N Sun, G T Li, L Cheng. Design and validation of a self-aligning index finger exoskeleton for post-stroke rehabilitation. *IEEE Transactions on Neural Systems and Rehabilitation Engineering*, 2021, 29: 1513-1523.
[38] J F Li, Q Cao, C Z Zhang, et al. Position solution of a novel four-DOFs self-aligning exoskeleton mechanism for upper limb rehabilitation. *Mechanism and Machine Theory*, 2019, 141: 14-39.
[39] J F Li, Q Cao, M J Dong, et al. Compatibility evaluation of a 4-DOF ergonomic exoskeleton for upper limb rehabilitation. *Mechanism and Machine Theory*, 2021, 156: 104146.
[40] E Trigili, S Crea, M Moisè, et al. Design and experimental characterization of a shoulder-elbow exoskeleton with compliant joints for post-stroke rehabilitation. *IEEE/ASME Transactions on Mechatronics*, 2019, 24(4): 1485-1496.
[41] A L Lenz, M A Strobel, A M Anderson, et al. Assignment of local coordinate systems and methods to calculate tibiotalar and subtalar kinematics: A systematic review. *Journal of Biomechanics*, 2021, 120: 110344.

[42] M Fukano, T Fukubayashi, T Kumai. In vivo talocrural and subtalar kinematics during the stance phase of walking in individuals with repetitive ankle sprains. *Journal of Biomechanics*, 2020, 101: 109651.
[43] X W Kong, C M Gosselin. Type synthesis of 4-DOF SP-equivalent parallel manipulators: A virtual chain approach. *Mechanism and Machine Theory*, 2006, 41(11): 1306-1319.
[44] Y W Li, L M Wang, J F Liu, et al. Applicability and generality of the modified Grübler-Kutzbach criterion. *Chinese Journal of Mechanical Engineering*, 2013, 26(2): 257-263.
[45] Z Huang, Q C Li. Type synthesis of symmetrical lower-mobility parallel mechanisms using the constraint-synthesis method. *The International Journal of Robotics Research*, 2003, 22(1): 59-79.

Ya Liu born in 1994 is currently a Ph.D. candidate at *School of Mechanical Engineering, Yanshan University, China*. His main research direction is rehabilitation robot.

Wenjuan Lu born in 1983 is currently an associate professor at *Dongguan University of Technology, China*. She received her Ph.D. degree in mechatronic engineering from *Yanshan University, China,* in 2015. Her research interests include parallel mechanism, type synthesis.

Dabao Fan born in 1993 is currently a postdoctoral at *Dongguan University of Technology, China*. He received his Ph.D. degree in mechanical engineering from *Yanshan University, China*, in 2023. His main research interests include mechanism synthesis and reconfigurable mechanism.

Weijian Tan born in 1999 is currently a graduate student at *School of Mechanical Engineering, Dongguan University of Technology, China*. His main research direction is rehabilitation robot.

Bo Hu born in 1982 is currently a professor at *Yanshan University, China*. He received his Ph.D. degree in mechatronic engineering from *Yanshan University, China,* in 2010. His research interests include theory and technology of parallel robot, mechanism theory and technology of super-redundant series–parallel hybrid robot.

Daxing Zeng born in 1978 is currently a professor at *Dongguan University of Technology, China*. He received his Ph.D. degree in mechatronic engineering from *Yanshan University, China,* in 2008. His research interests include theory of mechanism and machine, parallel mechanism, type synthesis and image processing.